The Role of Orbital Interactions in Determining the Interlayer Spacing in Graphite Slabs

Kazunari Yoshizawa,* Takashi Yumura, Tokio Yamabe, and Shunji Bandow

Contribution from the Department of Molecular Engineering, Kyoto University, Sakyo-ku, Kyoto 606-8501, Japan, Institute for Fundamental Chemistry, 34-4 Takano-Nishihiraki-cho, Sakyo-ku, Kyoto 606-8103, Japan, and Japan Science and Technology Corporation, Department of Materials Science and Engineering, Meijo University, Tenpaku-ku, Nagoya 468-8502, Japan

Received December 21, 1999. Revised Manuscript Received September 27, 2000

Abstract: The orbital interaction between the sheets of graphite slabs, in which small numbers of sheets (*n*) are stacked in the ABAB fashion, is theoretically analyzed. We predict from the nodal properties in the interlayer orbital interaction that the spacing between the graphite sheets should be large (small) when *n* is even (odd). Results from density functional theory calculations with gradient corrections are in good agreement with this theoretical prediction; optimized interlayer spacings show oscillatory behavior as a function of *n*. The interlayer spacing is predicted to be 3.58 and 3.30 Å when *n* is 2 and 3, respectively. The spacing in the double-layer slab is surprisingly large in comparison with the value of 3.35 Å observed in natural graphite. The significant features of the interlayer spacing in the graphite slabs are discussed in detail, with an emphasis on the aspect of frontier orbital ideas and orbital symmetry concepts.

Introduction

Three types of stacking are known to exist in graphite: the ABAB, ABCABC, and AAAA types.[1] The most common form of graphite has the ABAB stacking (the Bernal structure), and natural graphite also contains the ABCABC stacking (the rhombohedral structure) in a small ratio. In natural graphite, the C−C bond length is 1.42 Å within the sheets and the nearest-neighbor sheets are separated by 3.35 Å. The interlayer spacing is approximately the sum of the van der Waals radii of the carbon atom, and thus, it is widely accepted that the van der Waals interaction plays a dominant role in determining the layer structure of graphite. The AAAA stacking has not been observed so far in natural graphite, but it is common for graphite intercalation compounds (GICs) such as LiC_6 and KC_8.[1]

About two decades ago, Iijima reported from high-resolution transmission electron microscopy (TEM) observations that double sheets of graphitic carbon have extremely large interlayer spacings compared with those in crystalline regions that consist of a number of graphite sheets.[2] Reported large interlayer spacings for double-layer graphitic carbon up to 3.84 Å were proposed to be a consequence of the relaxation of van der Waals bonding between the sheets, due to crystalline defects and small cluster sizes. In 1991, Iijima discovered carbon nanotubes in a slaglike carbonaceous deposit grown on a negative electrode as a byproduct of fullerene-rich soot.[3] Several research groups have turned much attention to the interlayer spacing in multiwalled carbon nanotubes and graphitic nanoparticles.[4] Sun et al. reported from TEM measurements that large intershell spacings of multiwalled carbon nanotubes, denoted by $\hat{d}_{002}$, fall in the range from 3.59 to 3.62 Å.[5] This large intershell spacing is attributable to the large curvature of small-diameter nanotubes. A similar observation on the unusually large interlayer spacings that range up to 4 Å was made in the carbon material prepared from heat treatment of phenol−formaldehyde resin at ∼600 °C.[6] Moreover, Bandow et al. recently observed from X-ray diffraction measurements that the averaged spacing of the double-layer region between single-walled carbon nanohorns produced by the CO_2 laser ablation of carbon target is 4 Å.[7] Anomalous observations of the spacing in the double-layer regions in various carbon materials have been repeatedly reported so far, but our knowledge on the triple-, quadruple-, and quintuple-layer regions is still lacking.

In previous work,[8−10] we investigated preferred structural changes in one-dimensional and two-dimensional electronic systems by analyzing the transition density[11] between two bands in the vicinity of the Fermi level, specifically for the bond-length alternation of polyacene and the layer structures of

* To whom all correspondence should be addressed at Kyoto University. E-mail: kazunari@scl.kyoto-u.ac.jp.

(1) (a) Dresselhaus, M. S.; Dresselhaus, G. *Adv. Phys.* **1981**, *30*, 139. (b) *Graphite Intercalation Compounds*; Nakao, K., Solin, S. A., Eds.; Elsevier: Lausanne, 1985. (c) Dresselhaus, M. S.; Dresselhaus, G.; Sugihara, K.; Spain, I. L.; Goldberg, H. A. *Graphite Fibers and Filaments*; Springer: Berlin, 1988. (d) Brandt, N. B.; Chudinov, S. M.; Ponomarev, Y. G. *Semimetals 1. Graphite and Its Compounds*; Elsevier: Amsterdam, 1988. (e) *Graphite Intercalation Compounds I*; Zabel, H., Solin, S. A., Eds.; Springer: Berlin, 1990. (f) *Graphite Intercalation Compounds II*; Zabel, H., Solin, S. A., Eds.; Springer: Berlin, 1992.

(2) Iijima, S. *Chem. Scr.* **1978−79**, *14*, 117.

(3) Iijima, S. *Nature* **1991**, *354*, 56.

(4) (a) Saito, Y.; Yoshikawa, T.; Bandow, S.; Tomita, M.; Hayashi, T. *Phys. Rev. B* **1993**, *48*, 1907. (b) Iijima, S. *MRS Bull.* **1994**, *19*, 43. (c) Bretz, M.; Demczyk, B. G.; Zhang, L. *J. Cryst. Growth* **1994**, *141*, 304. (d) Andersson, O. E.; Prasad, B. L. V.; Sato, H.; Enoki, T.; Hishiyama, Y.; Kaburagi, Y.; Yoshikawa, M.; Bandow, S. *Phys. Rev. B* **1998**, *58*, 16387.

(5) Sun, X.; Kiang, C.-H.; Endo, M.; Takeuchi, K.; Furuta, T.; Dresselhaus, M. S. *Phys. Rev. B* **1996**, *54*, 12629.

(6) Tanaka, K.; Ueda, M.; Koike, T.; Yamabe, T.; Yata, S. *Synth. Met.* **1988**, *25*, 265.

(7) Bandow, S.; Kokai, F.; Takahashi, K.; Yudasaka, M.; Qin, L. C.; Iijima, S. *Chem. Phys. Lett.* **2000**, *321*, 514.

(8) Yoshizawa, K.; Hoffmann, R. *J. Chem. Phys.* **1995**, *103*, 2126.

(9) (a) Yoshizawa, K.; Kato, T.; Yamabe, T. *J. Chem. Phys.* **1996**, *105*, 2099. (b) Yoshizawa, K.; Kato, T.; Yamabe, T. *Bull. Chem. Soc. Jpn.* **1998**, *71*, 2087.

(10) Yoshizawa, K.; Yumura, T.; Yamabe, T. *J. Chem. Phys.* **1999**, *110*, 11534.

10.1021/ja994457o CCC: $19.00
Published on Web 11/11/2000

graphite and arsenic. The preferred structures in these extended systems can be viewed as second-order perturbation effects. We examined in detail the interlayer interactions in graphite and GICs and proposed that the ABAB stacking in graphite should be a consequence of the orbital interaction between the nearest-neighbor sheets rather than of generally accepted van der Waals interaction.

The issue that we address in this paper is how the interlayer spacing is affected in graphite slabs that consist of small numbers of sheets. The present work is an extension of our previous studies on the interlayer orbital interaction in graphite.[9] We discuss here significant nanometer-sized electronic features of the interlayer spacing in the graphite slabs, with an emphasis on the aspect of frontier orbital ideas and orbital symmetry concepts.[12−14]

Interlayer Spacing in Graphite Slabs. We optimized the structure of two-dimensional graphite slabs in which small numbers (n) of sheets are stacked in the ABAB manner. The purpose of our calculations is to look in detail at how the interlayer spacing changes as the thickness of the graphite slabs increases from $n = 2$. Trickey et al. reported from local density approximation (LDA) calculations that the spacing of a double-layer model is only 2% expanded in comparison with that of bulk graphite.[15] However, such LDA calculations have a general tendency to underestimate interatomic distances in molecules and solids. Perdew et al. demonstrated that generalized gradient approximation (GGA)[16] calculations are more accurate than local spin density approximation calculations with respect to many electronic properties. We thus employed a density functional theory (DFT) method with gradient corrections in this study. We applied a pseudopotential total-energy method,[17] with CASTEP version 3.0. The wave functions of valence electrons were expanded in a basis set of plane wave with an energy cutoff 600 eV. We used norm-conserving pseudopotentials in the Kleinman−Bylander representation[18] optimized using the scheme of Lin et al.[19] CASTEP approximates several integrals by numerical summation over a finite number of k points on the basis of the Monkhorst−Pack scheme.[20] We used an 18k-point set, which is sufficient to describe the band structure of graphite according to ref 15 and a supercell of $2.46 \times 2.46 \times 50$ Å^3. The empty space between slabs is more than 30 Å even in the thickest slab of $n = 7$, being large enough to neglect the interaction between slabs. The accuracy of the computational scheme was tested from calculations for bulk graphite with the ABAB and AAAA stacking modes; the ABAB stacking is 0.05 eV/unit cell (C_4) more stable than the AAAA stacking. This DFT method predicted the interlayer spacing of bulk graphite with the ABAB stacking to be 3.26 Å, which is in good agreement with the observed value of 3.35 Å. Thus, the method of choice is appropriate for our purpose.

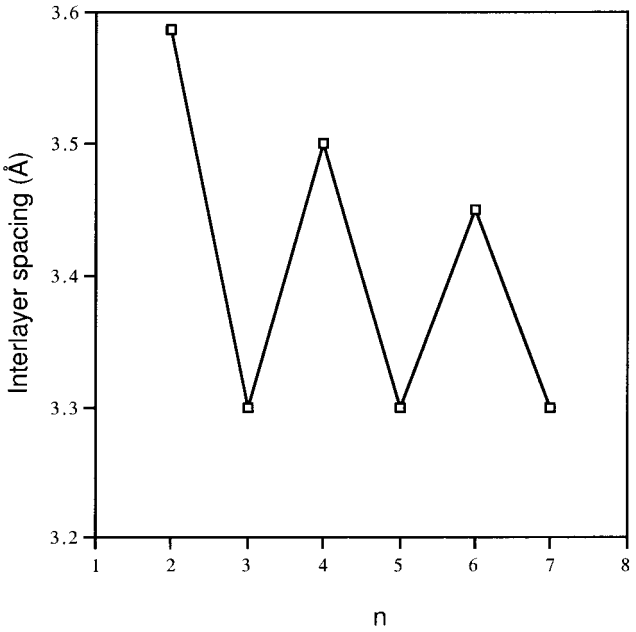

Figure 1. Optimized interlayer spacings for the graphite slabs in which small numbers (n) of graphite sheets are stacked in the ABAB fashion.

Calculated spacings are plotted as a function of n in Figure 1; they show oscillatory behavior as the thickness of the slabs changes. No constraint of interlayer spacings was assumed for $n \geq 2$. The variation in optimized interlayer spacings in a single-slab model was very small, the values falling in the error range of the plotted squares. The interlayer spacing is large (small) when n is even (odd). This is an interesting nanometer-sized electronic effect that we do not intuitively expect. In particular, when n is 2, the interlayer spacing is surprisingly large (3.58 Å), but when n is 3, it is small (3.30 Å). In odd-numbered graphite slabs, the calculated spacings are close to that of bulk graphite. Clearly, the large spacings in the even-numbered graphite slabs do not result from nonperiodic effects such as crystalline defects and small cluster sizes because these models are perfect two-dimensional systems. We believe that this significant structural feature should derive from the intrinsic orbital nature of even-numbered graphite slabs.

Orbital Interactions in Graphite Slabs. To understand the interesting size effect on the interlayer spacing in the graphite slabs, let us consider interlayer orbital interactions between the graphite sheets. General features of the orbital interactions in graphite are seen in a quantum chemistry textbook.[21] The interlayer orbital interactions in graphite are weak compared with those within the sheet, but not negligible.[22] The graphite-to-diamond high-pressure reaction was analyzed by Kertesz and Hoffmann in terms of interlayer orbital interactions.[23] Taking these into account, we consider essential orbital features that determine the interlayer interactions in the graphite slabs that consist of small numbers of sheets stacked in the ABAB manner as shown in Figure 2.

(11) Transition density is a beautiful concept written with perturbation theory by Longuet-Higgins, Bader, and Pearson: (a) Longuet-Higgins, H. C. *Proc. R. Soc. A* **1956**, *235*, 537. (b) Bader, R. F. W. *Mol. Phys.* **1960**, *3*, 137. (c) Bader, R. F. W. *Can. J. Chem.* **1962**, *40*, 1164. (d) Bader, R. F. W. *Atoms in Molecules*; Clarendon: Oxford, 1994. (e) Pearson, R. G. *J. Am. Chem. Soc.* **1969**, *91*, 4947. (f) Pearson, R. G. *J. Chem. Phys.* **1970**, *52*, 2167. (g) Pearson, R. G. *Acc. Chem. Res.* **1971**, *4*, 152.

(12) Fukui, K. *Theory of Orientation and Stereoselection*; Springer-Verlag: Berlin, 1975.

(13) Woodward, R. B.; Hoffmann, R. *The Conservation of Orbital Symmetry*; Verlag Chemie GmbH: Weinheim, 1970.

(14) Albright, T. A.; Burdett, J. K.; Whangbo, M.-H. *Orbital Interactions in Chemistry*; Wiley: New York, 1985.

(15) Trickey, S. B.; Müller-Plathe, F.; Diercksen. G. H. F.; Boettger. J. C. *Phys Rev. B* **1992**, *45*, 4460.

(16) (a) Perdew, J. P.; Yue, W. *Phys Rev. B* **1986**, *33*, 8800. (b) Perdew, J. P.; Chevary, J. A.; Vosko, S. H.; Jackson, K. A.; Pederson, M. R.; Singh, D. J.; Fiolhais, C. *Phys Rev. B* **1992**, *46*, 6671.

(17) Payne, M. C.; Teter, M. P.; Allan, D. C.; Arias, T. A.; Joannopoulos, J. D. *Rev. Mod. Phys.* **1992**, *64*, 1045.

(18) Kleinman, L.; Bylander, D. M. *Phys Rev. Lett.* **1980**, *48*, 566.

(19) Lin, L. S.; Qteish, A.; Payne, M. C.; Heine, V. *Phys Rev. B* **1993**, *47*, 4174.

(20) Monkhorst, H. J.; Pack, J. D. *Phys Rev. B* **1976**, *13*, 5188. *Cerius 2*, Version 3.0; Molecular Simulations Inc.: San Diego, CA, 1997.

(21) Lowe, J. P. *Quantum Chemistry*, 2nd ed.; Academic Press: Boston, MA, 1993.

(22) Burdett, J. K. *Chemical Bonding in Solids*; Oxford University: New York, 1995.

(23) Kertesz, M.; Hoffmann, R. *J. Solid State Chem.* **1984**, *54*, 313.

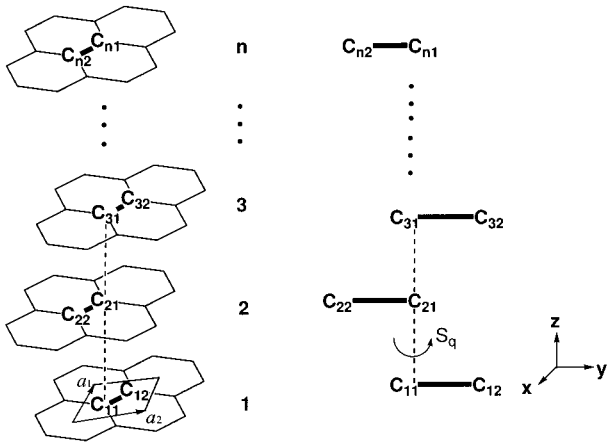

Figure 2. Schematic representation for the graphite slab in which *n* sheets are stacked in the ABAB fashion.

The *j*th molecular orbital of an isodistant one-dimensional chain in which each atom has an atomic orbital χ_q is written within the framework of the Hückel approximation as

$$\psi_j = \sqrt{\frac{2}{n+1}} \sum_{q=1}^{n} \sin\left(\frac{\pi jq}{n+1}\right)\chi_q \qquad (1)$$

where *n* is the number of atoms that constitute the chain. Equation 1 is applicable to the description of the wave function for the unit cell of the graphite slab. Let us next consider the orbitals of a single graphite sheet. Since the unit cell of a single graphite sheet consists of two carbon atoms, the unit cell of the *n*-layer graphite slab has 2*n* carbon atoms in it. It is the carbon ladder chain indicated in the right of Figure 2. The bonding and the antibonding orbitals for the C_2 unit in the *q*th sheet are

$$\varphi_q^b = \sqrt{\frac{1}{2}}(\phi_{q1} + \phi_{q2}) \qquad (2)$$

and

$$\varphi_q^a = \sqrt{\frac{1}{2}}(\phi_{q1} - \phi_{q2}) \qquad (3)$$

respectively. Here we confined our discussion to the π bands, and ϕ_{q1} and ϕ_{q2} are therefore the $2p_z$ atomic orbitals at the 1 and 2 sites in the C_2 unit cell, respectively. We took the *z* axis as the stacking direction. From these expressions, the bonding and the antibonding orbitals, with respect to the nearest-neighbor C−C bond, for the carbon ladder chain indicated in the right of Figure 2 can be written as

$$\psi_j^b = \sqrt{\frac{2}{n+1}} \sum_{q=1}^{n} \sin\left(\frac{\pi jq}{n+1}\right)\varphi_q^b = \sqrt{\frac{1}{n+1}} \sum_{q=1}^{n} \sin\left(\frac{\pi jq}{n+1}\right) \times \{\phi_1(S_q z - qa_z) + \phi_2(S_q z - qa_z)\} \quad (1 \le j \le n) \quad (4)$$

and

$$\psi_j^a = \sqrt{\frac{2}{n+1}} \sum_{q=1}^{n} \sin\left(\frac{\pi jq}{n+1}\right)\varphi_q^a = \sqrt{\frac{1}{n+1}} \sum_{q=1}^{n} \sin\left(\frac{\pi jq}{n+1}\right) \times \{\phi_1(S_q z - qa_z) - \phi_2(S_q z - qa_z)\} \quad (5)$$

respectively, where a_z is the translation vector along the *z* axis and S_q is the screw axis operator[24] that rotates the orientation of a unit cell by 180° with respect to the neighbor unit cells. This operator can be conveniently used for our theoretical analysis on the ABAB stacking of graphite sheet, leading to the reduction of the size of unit cell. We took the *z* axis as the screw axis.

Hence, the crystal orbitals for the graphite slab indicated in the left of Figure 2 can be written as

$$\psi_{k_1,k_2,j}^b = \frac{1}{\sqrt{N(n+1)}} \sum_{q=1}^{n} \sum_{\upsilon_1} \sum_{\upsilon_2} e^{i(k_1\upsilon_1 a_1 + k_2\upsilon_2 a_2)} \sin\left(\frac{\pi jq}{n+1}\right) \times \{\phi_1(x_1 - \upsilon_1 a_1, x_2 - \upsilon_2 a_2, S_q z - qa_z) + \phi_2(x_1 - \upsilon_1 a_1, x_2 - \upsilon_2 a_2, S_q z - qa_z)\} \quad (6)$$

and

$$\psi_{k_1,k_2,j}^a = \frac{1}{\sqrt{N(n+1)}} \sum_{q=1}^{n} \sum_{\upsilon_1} \sum_{\upsilon_2} e^{i(k_1\upsilon_1 a_1 + k_2\upsilon_2 a_2)} \sin\left(\frac{\pi jq}{n+1}\right) \times \{\phi_1(x_1 - \upsilon_1 a_1, x_2 - \upsilon_2 a_2, S_q z - qa_z) - \phi_2(x_1 - \upsilon_1 a_1, x_2 - \upsilon_2 a_2, S_q z - qa_z)\} \quad (7)$$

where k_1 and k_2 are the wave vectors and a_1 and a_2 are the translation vectors that generate the lattice points on the graphite sheets.

We found that the sine term of eqs 6 and 7 plays a dominant role in determining the interlayer interactions in the graphite slabs. When *n* is odd (= 2*m* +1), both the bonding and the antibonding orbitals of $j = (n + 1)/2 = m + 1$ have a node on every even numbered sheet because of the following relation:

$$\sin\left(\frac{\pi jq}{n+1}\right) = \sin\left(\frac{\pi q}{2}\right) = 0 \quad (q = 2, 4, 6, ...) \qquad (8)$$

In such a case, there is no orbital amplitude on every even-numbered sheet. Figure 3 shows the bonding and the antibonding orbitals for the unit cell of the triple-layer slab, from which we can qualitatively derive crystal orbitals at any *k* point using eqs 6 and 7. When *j* is 3, the interaction between the sheets is in phase, but when *j* is 1, there is always a node between the sheets. In this way, the number of nodes in the orbitals increases with a decrease in *j* with respect to interlayer coupling since the 2p atomic orbital has a node. There is a nice analogy between these orbitals and wave functions of a particle in a box, as indicated. As shown in Figure 3, the orbitals of $j = 2$ have a node exactly on the central sheet and can be viewed as a kind of nonbonding orbital; thus, in these orbitals, there is no net interaction between the nearest-neighbor sheets. However, note that the second-nearest-neighbor interaction is in phase in these nonbonding orbitals. On the other hand, when *n* is even, such a nonbonding orbital does not appear, due to symmetry restriction. Figure 4 shows the bonding and the antibonding orbitals for the unit cell of the double-layer graphite slab. When *j* is 2, the interaction between the graphite sheets is in phase, but when *j* is 1, there is a node between the sheets.

We know that frontier orbital ideas and simple concepts of orbital symmetry[12−14] are applicable to the understanding of molecular and crystal structures. In those arguments, most of the responsibility for chemical structure and reactivity is placed on a subset of frontier orbitals and their symmetries. So let us next turn our attention to the orbitals of the graphite slabs in the vicinity of the Fermi level. What we use here is

(24) (a) Imamura, A. *J. Chem. Phys.* **1970**, *52*, 3168. (b) Kollmar, C.; Hoffmann, R. *J. Am. Chem. Soc.* **1990**, *112*, 8230.

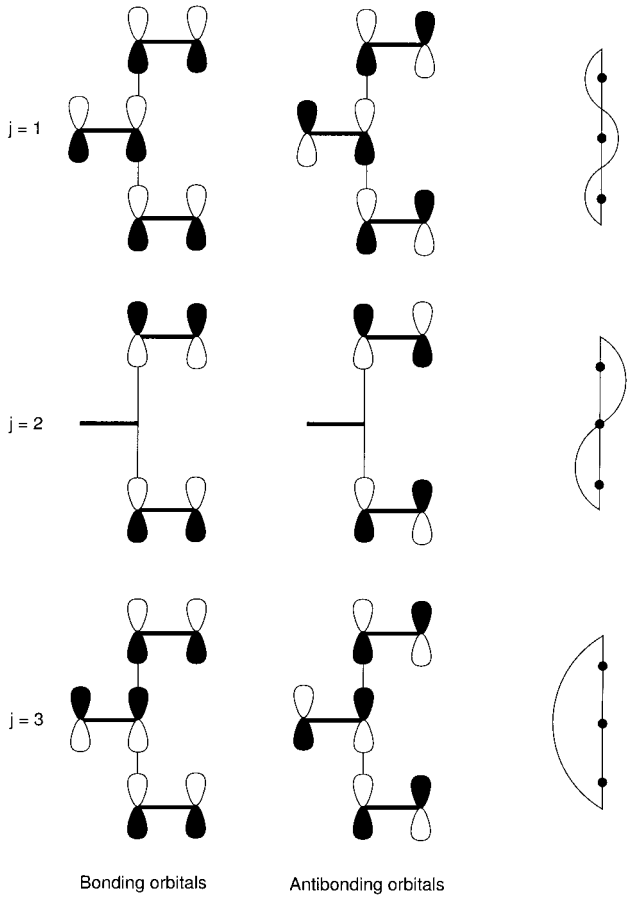

Figure 3. Bonding and the antibonding orbitals for the unit cell of the triple-layer graphite slab.

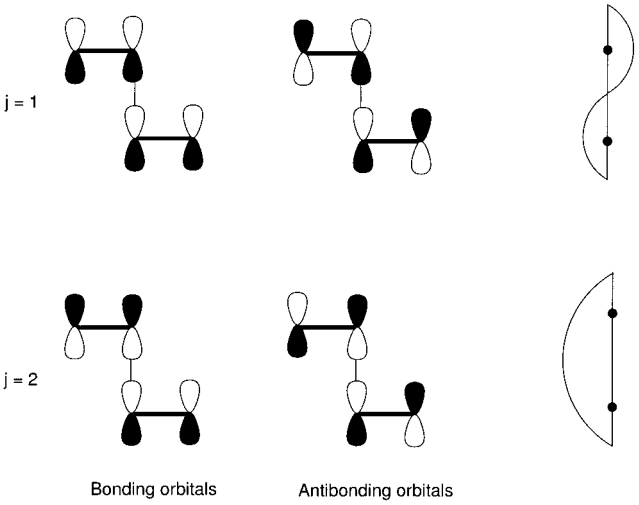

Figure 4. Bonding and the antibonding orbitals for the unit cell of the double-layer graphite slab.

the extended Hückel method,[25] which models general orbital energy trends, band gaps, orbital interactions, and major charge shifts well. Parameters used for the carbon atom are $H_{ii} = -21.4$ eV and $\zeta = 1.625$ for the 2s atomic orbital, and $H_{ii} = -11.4$ eV and $\zeta = 1.625$ for the $2p_x$, $2p_y$, and $2p_z$ atomic orbitals, in which H_{ii} and ζ are the orbital energies and the Slater exponents, respectively. A 400*k*-point set was adopted for the band structure calculations with respect to a symmetry line, and lattice sums were taken to the fifth-nearest neighbors. These

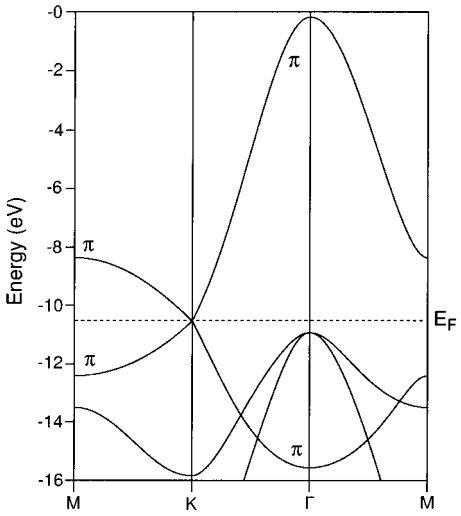

Figure 5. Band electronic structure for the single graphite sheet from extended Hückel calculations. E_F indicates the Fermi level.

extended Hückel calculations were performed with YAeHMOP.[26]

The well-known band electronic structure for the single graphite sheet is shown in Figure 5. The unit cell of the graphite sheet consists of two carbon atoms, and accordingly there are two π bands as indicated, the π bands being crossed at the point K ($2\pi/(3a_1)$, $2\pi/(3a_2)$). Note that the Fermi wavenumber k_F lies at this important symmetry point.

Figure 6 shows the band electronic structures for the double- and triple-layer slabs, in which the screw axis operator is not used; we see four π bands in the double-layer slab and six π bands in the triple-layer slab. These π bands are significantly split into the bonding and the antibonding sets at the point Γ (0, 0), but these bands are nearly degenerate at the point K. Since the k_F of the graphite sheet lies at this symmetry point, the shapes and energies of the crystal orbitals in the vicinity of the point K should play a dominant role in determining preferred layer structures of the graphite slabs.

The highest occupied crystal orbital (HOCO) and the next highest occupied crystal orbital (HOCO-1) at the point K in the double- and triple-layer slabs from extended Hückel calculations are shown in Figure 7. The "highest occupied state" may be more appropriate for condensed matter physicists. These crystal orbitals can also be generated from Figures 2 and 3, according to eqs 6 and 7. The HOCO in the double-layer slab is out of phase while the HOCO-1 is in phase, with respect to the interlayer coupling. This orbital feature could lead to a significant effect on the layer structure. In the HOCO, there is a node at the center of the two sheets. Such a nodal property results in removal of electron density from this region of space,[14] and the two graphite sheets would experience repulsive force if this orbital is occupied. We therefore expect that the spacing in the double-layer slab should become large.

The state of affairs is a little different in the triple-layer graphite slab. The HOCO and the HOCO-1 are substantially degenerate at the point K. Thus, not only the HOCO but also the HOCO-1 can play a dominant role in determining the spacing in the triple-layer slab. The HOCO has a node between the sheets, whereas the HOCO-1 has no orbital amplitude on the central sheet. This interesting orbital character is a consequence of the sine term in eq 6, and this is valid for all odd-numbered graphite slabs. The antibonding nature of the HOCO

(25) (a) Hoffmann, R. *J. Chem. Phys.* **1963**, *39*, 1397. (b) Hoffmann, R.; Lipscomb, W. N. *J. Chem. Phys.* **1962**, *36*, 2179; **1962**, *37*, 2872.

(26) Landrum. G. *YAeHMOP* (Yet Another Extended Hückel Molecular Orbital Package), Version 2.0; Cornell University: Ithaca, NY, 1997.

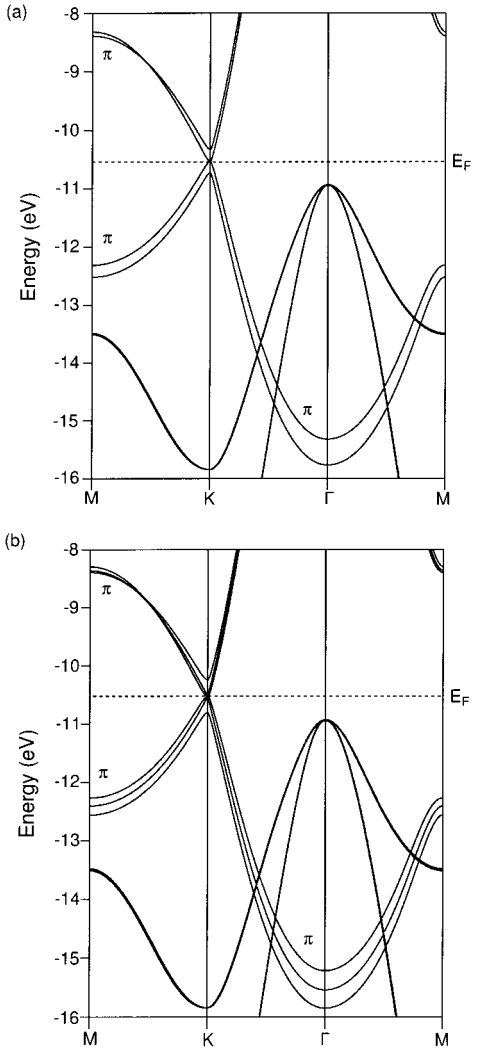

Figure 6. Band electronic structures for the (a) double- and (b) triple-layer graphite slabs from extended Hückel calculations. The interlayer spacings are 3.35 Å.

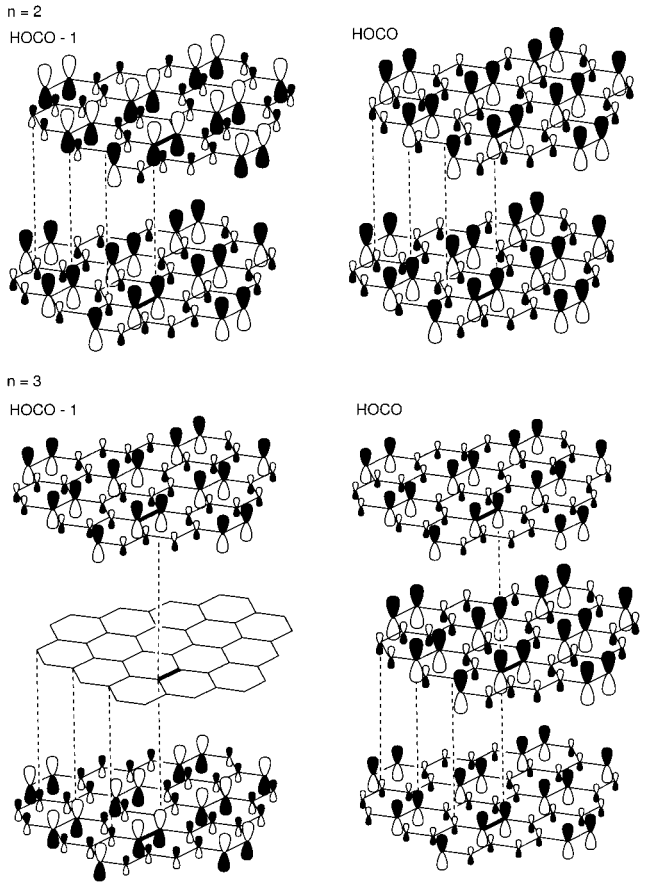

Figure 7. Highest occupied crystal orbital (HOCO) and next highest occupied crystal orbital (HOCO-1) at the point K in the double- and triple-layer graphite slabs.

can increase the interlayer spacing, while the nonbonding nature of the HOCO-1 can lead to the weakening of the repulsive interaction caused by the HOCO. Considering the different electronic features of the HOCO and the HOCO-1, the interlayer spacing should be small in the triple-layer slab in comparison with that in the double-layer slab. The computational results we have shown in the previous section are fully consistent with our qualitative orbital interaction analyses.

Concluding Remarks

We have considered the orbital interaction between the sheets of the graphite slabs, in which small numbers of sheets (*n*) are stacked in the ABAB fashion. We predicted from the nodal properties in the interlayer orbital interaction that the interlayer spacing should be large (small) when *n* is even (odd). Results from band electronic calculations of DFT type were in good agreement with this theoretical prediction. Optimized spacings showed oscillatory behavior as a function of *n*. The interlayer spacings were computed to be 3.58 and 3.30 Å when *n* is 2 and 3, respectively. The value in the double-layer slab is surprisingly large in comparison with 3.35 Å observed in the crystalline region of natural graphite. These are intrinsic features in the double- and triple-layer graphite slabs. The significant features of the interlayer spacing in the graphite slabs were derived from frontier orbital ideas and orbital symmetry concepts.

Acknowledgment. This work was supported by the "Research for the Future" Program from the Japan Society for the Promotion of Science (JSPS-RFTF96P00206) and by Grant-in-Aids for Scientific Research on the Priority Areas "Carbon Alloys" and "Molecular Physical Chemistry" from the Ministry of Education, Science, Sports and Culture of Japan.

JA994457O